

Article

Dynamic Analysis of the Switched-Inductor Buck-Boost Converter Based on the Memristor

Yan Yang, Dongdong Li * and Dongqing Wang

College of Electrical Engineering, Qingdao University, Qingdao 266000, China; yyang@qdu.edu.cn (Y.Y.); dqwang64@qdu.edu.cn (D.W.)

* Correspondence: 2019020694@qdu.edu.cn

Abstract: The direct current (DC)–DC converter presents abundant nonlinear phenomena, such as periodic bifurcation and chaotic motion, under certain conditions. For a switched-inductor buck-boost (SIBB) converter with the memristive load, this paper constructs its state equation model under two operating statuses, investigates its chaotic dynamic characteristics, and draws and analyzes the bifurcation diagrams of the inductive current and phase portraits, under some parameter changing by the MATLAB simulation based on the state equation. Then, by applying certain minor perturbations to parameters, the chaotic phenomenon suppression method is explored by controlling peak current in continuous current mode (CCM) to keep the converter run normally. Finally, the power simulation (PSIM) verifies that the waveforms and the phase portraits controlling the corresponding parameters are consistent with those of the MATLAB simulation.

Keywords: memristor; bifurcation; chaos; switched-inductor; buck-boost converter



check for updates

Citation: Yang, Y.; Li, D.; Wang, D. Dynamic Analysis of the Switched-Inductor Buck-Boost Converter Based on the Memristor. *Electronics* **2021**, *10*, 452. <https://doi.org/10.3390/electronics10040452>

Academic Editors: Christos Volos, Lazaros Moysis, Denis Butusov and Ahmed Radwan

Received: 7 January 2021

Accepted: 6 February 2021

Published: 11 February 2021

Publisher's Note: MDPI stays neutral with regard to jurisdictional claims in published maps and institutional affiliations.



Copyright: © 2021 by the authors. Licensee MDPI, Basel, Switzerland. This article is an open access article distributed under the terms and conditions of the Creative Commons Attribution (CC BY) license (<https://creativecommons.org/licenses/by/4.0/>).

1. Introduction

Power electronic technology has developed rapidly in recent years. Like other power electronic devices, the DC–DC converter has also penetrated into many fields, including energy science [1], physics [2], industry [3], automation [4–6], and so on.

The DC–DC buck-boost converter presents nonlinear physical phenomena, such as chaos and periodic motion, which are affected by system parameters, topological structure, load, and pulse period. The converter may produce results that cannot be predicted, and which affect the normal operation of the system. Thus, researchers from all over the world in this field pay lots of attention on these nonlinear phenomena. The bifurcation and chaos of a current-mode buck-boost converter was studied by using the input voltage, the reference current, and the load resistance as variable parameters [7]. The chaotic behavior in a Buck-Boost converter depending on the circuit parameters and the inductive load has been explored [8]. The chaos suppression for a Buck converter with the memristive load has also been investigated [9].

In recent years, some scientists have proposed a new switched-inductor topology [10]. It can be embedded into the DC–DC converter to replace the traditional inductor, forming a converter with stronger capacity of lifting and reducing voltage. One paper [11] studied the nonlinear phenomena in the switched-inductor buck-boost (SIBB) converter in continuous current mode (CCM). Another [12] investigated the various nonlinear behaviors of the SIBB converter under the resistive load in discontinuous current mode (DCM). A further study [13] has discussed chaos and its control of the current-mode switched-inductor converter. Lastly, another part of the literature [14] indicated that the SIBB converter can shift from DCM to CCM, and can operate in steady period-one state by utilizing ramp compensation.

The above results are mainly focused on the DC–DC converter with a normal load, without considering the memristive load. Similar to resistors, capacitors, and inductors, memristors are also two-terminal circuit elements, but are memristive. As the fourth

circuit element, the memristor has become an important research field, due to its wide application, such as in the fields of memory [15–18], artificial intelligence computers [19,20], and electronic engineering [21–32]. In the electronic engineering field, memristor has been used in logic-based digital operations [21,22] and analog circuits [23–26]; memristors also have been used in reconfigurable analog circuits as programmable elements [27,28], as filter elements for signal processing [29,30], and in power converters as memristive loads [31,32].

Recently, replacing the traditional load in boost and buck-boost converters with the memristors, and analyzing the nonlinear dynamic characteristics of converters, has become a hot topic [33]. However, few researchers consider the dynamic characteristics of the SIBB converter with the memristive load. The purpose of this paper is to investigate the bifurcation and chaotic behavior of the SIBB converter with the memristive load when the peak current changes. Furthermore, the harmful bifurcation and chaotic behavior are suppressed by controlling the peak current.

2. Working Principle of the Converter and the Memristor

Terminology description is given as follows.

SIBB	Switched-inductor buck-boost
CCM	Continuous current mode
DCM	Discontinuous current mode
DC	Direct current
PSIM	Power simulation
MATLAB	Matrix laboratory
PV	Photovoltaic
BAM	Bidirectional associative memory
AMS	Analog mixed signal
CNN	Cellular nonlinear/neural network
CT	Continuous-time
FIR	Finite impulse response

2.1. Working Principle of the Converter

The current-mode-controlled SIBB converter is a kind of DC–DC converter controlled by the inductive current. It is formed by applying a switched-inductor structure to the traditional converter. Its basic circuit is shown in Figure 1.

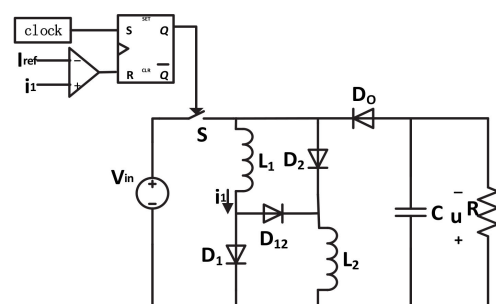


Figure 1. The switched-inductor buck-boost (SIBB) converter under peak current mode.

The feedback loop consists of an RS flip-flop and a comparator. An RS flip-flop has a reset input R and a set input S , as well as an output Q . The output Q directly controls the state of the switch S . The set input S comes from the clock, while the reset input R comes from the comparison of the reference current I_{ref} and the inductive current i_l in the comparator. This converter has two operating modes: continuous current mode (CCM) and discontinuous current mode (DCM). This paper studies the dynamic characteristics of the converter in CCM. In this mode, the circuit has two statuses, as shown in Figure 2.

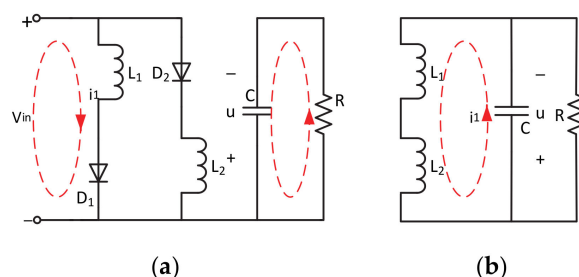


Figure 2. Circuit statuses in continuous current mode (CCM). (a) Switch *S* is ON. (b) Switch *S* is OFF.

To make the analysis easier, let two inductors of the switched-inductor $L_1 = L_2$ and i_1 is approximately equal to i_2 , and the inductive current i_2 can be written as i_1 . Thus, the system with the resistive load can be simplified to a second-order model, and its state equations are as follows

$$\begin{cases} \dot{x} = A_1x + B_1V_{in} & S \text{ is ON} \\ \dot{x} = A_2x + B_2V_{in} & S \text{ is OFF} \end{cases} \quad (1)$$

where $x = [i_1 \quad u]^T$ is the state vector, V_{in} is the input voltage, and the coefficient matrices are

$$A_1 = \begin{bmatrix} 0 & 0 \\ 0 & -\frac{1}{RC} \end{bmatrix}, B_1 = \begin{bmatrix} \frac{1}{L_1} \\ 0 \end{bmatrix}, A_2 = \begin{bmatrix} 0 & -\frac{1}{2L_1} \\ \frac{1}{C} & -\frac{1}{RC} \end{bmatrix}, B_2 = \begin{bmatrix} 0 \\ 0 \end{bmatrix}$$

2.2. The Simulation Model of the Memristor

About 50 years ago, professor Cai theoretically predicted that the existence of a nonlinear, passive, two-terminal electronic element that could describe the relationship between charge and flux, and called it a memristor [34]. Cai also generated the concept of a generalized memristor. In 2008, the feasibility of memristors was reported in *Nature*. This report shocked the international electrical and electronic world, and made the theoretical basis of circuits more perfect. The memristor was finally unveiled in 2009 after a flurry of research by many scientists. Its symbol is shown in Figure 3.

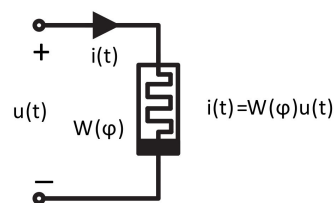


Figure 3. Symbol of the memristor.

Memristors are similar to resistors, capacitors, and inductors as a nonlinear, passive, two-terminal electronic element. It has two forms: the charge-controlled memristor and the magnetron-controlled memristor. The relationship between its magnetic flux and accumulated charge is

$$M(q) = \frac{d\varphi(q)}{dq} \quad (2)$$

$$W(\varphi) = \frac{dq(\varphi)}{d\varphi} \quad (3)$$

where $M(q)$ is called memristance and $W(\varphi)$ is called memductance [34].

A simulator of the magnetron-controlled memristor is designed by using circuit elements, as shown in Figure 4.

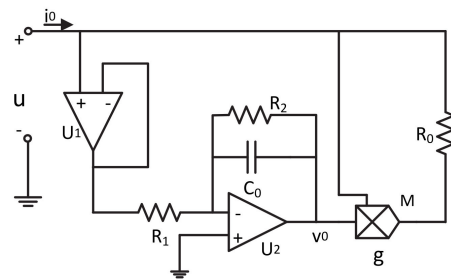


Figure 4. The simulator of the magnetron-controlled memristive load.

Referring to [33], the simulation circuit consists of two operational amplifiers, U_1 and U_2 ; three resistors, R_1 , R_2 , and R_0 ; a capacitor C_0 ; and a multiplier M , which is $g = -0.1$. In addition, u and i_0 are expressed as the input voltage and input current of the simulation circuit, respectively. According to the volt-ampere relationship of the memristor, $u(t) = M(q)i(t)$ and $i(t) = W(\varphi)u(t)$. The mathematical model of the memristor simulator can be obtained as follows:

$$i_0 = \frac{1}{R_0}(1 - gv_0)u \tag{4}$$

$$\frac{dv_0}{dt} = -\frac{1}{R_1C_0}u - \frac{1}{R_2C_0}v_0 \tag{5}$$

3. The Modeling and Simulation

3.1. The Modeling of the SIBB Converter with the Memristive Load

We have described the operating principle of the SIBB converter and obtained its state equations under the resistive load. Now we have replaced the resistive load with the memristive load.

In CCM, the SIBB converter with its memristive load still has two statuses: switch S is on, D_0 is off; and switch S is off, D_0 is on, as shown in Figure 2. At this time, the voltage on the capacitor C is the input voltage of the simulation circuit, and i_0 is the input current of the simulation circuit. The state equations of the system with the memristive load can be obtained as follows:

$$\begin{cases} \dot{x} = A_1x + B_1V_{in} + Cy & S \text{ is ON} \\ \dot{x} = A_2x + B_2V_{in} + Cy & S \text{ is OFF} \end{cases} \tag{6}$$

where $x = [i_1 \quad u \quad v_0]^T$ is the state vector; V_{in} is the input voltage; and y is the product of two state variables, such that $y = uv_0$. The coefficient matrices are

$$A_1 = \begin{bmatrix} 0 & 0 & 0 \\ 0 & -\frac{1}{R_0C} & 0 \\ 0 & \frac{1}{R_1C_0} & -\frac{1}{R_2C_0} \end{bmatrix}, B_1 = \begin{bmatrix} \frac{1}{L_1} \\ 0 \\ 0 \end{bmatrix},$$

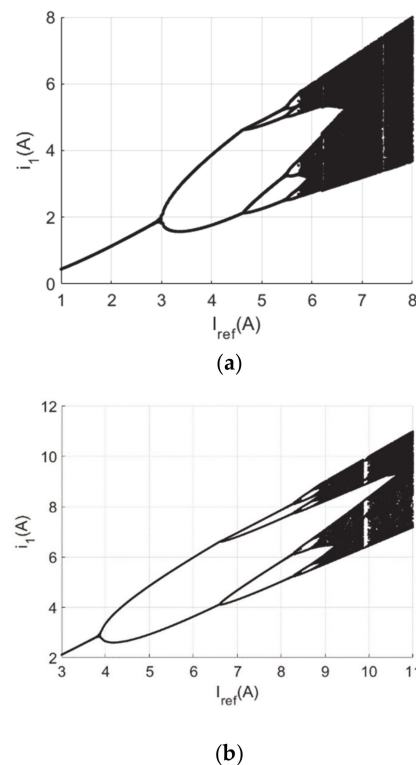
$$C = \begin{bmatrix} 0 \\ \frac{g}{R_0C} \\ 0 \end{bmatrix}, A_2 = \begin{bmatrix} 0 & -\frac{1}{2L_1} & 0 \\ \frac{1}{C} & -\frac{1}{R_0C} & 0 \\ 0 & \frac{1}{R_1C_0} & -\frac{1}{R_2C_0} \end{bmatrix}, B_2 = \begin{bmatrix} 0 \\ 0 \\ 0 \end{bmatrix}$$

3.2. The Simulation of the SIBB Converter with the Memristive Load

The circuit parameters are selected as shown in Table 1. Taking I_{ref} as the bifurcation parameter, the bifurcation diagrams of the inductive current i_1 with I_{ref} changing can be obtained, as shown in Figure 5. Figure 5a is the bifurcation diagram of the SIBB converter with the resistive load, and Figure 5b is the bifurcation diagram of the SIBB with the memristive load.

Table 1. The circuit element parameters.

Elements	Parameters	Values
Voltage	V_{in}	5 V
Inductor	L_1, L_2	0.1 mH
Capacitor	C	10 μ F
Capacitor	C_0	20 nF
Resistor	R_1, R_2	1 k Ω
Resistor	R, R_0	5 Ω
Frequency	f	20 kHz
Multiplier	g	-0.1

**Figure 5.** The bifurcation diagram of inductive current i_1 controlled by the reference current I_{ref} . (a) With the resistive load, (b) With the memristive load.

According to the comparison of the bifurcation diagrams, we can see that the memristive load does not affect the bifurcation structure. Both of them have chaos and bifurcation of two-period, four-period, eight-period, etc., but the bifurcation point of the period doubling can be moved. The results are listed as follows:

- (1) The two-period bifurcation of the converter with the resistive load occurs when $I_{ref} = 3$ A, while two-period bifurcation of the converter with the memristive load occurs when $I_{ref} = 3.85$ A. Therefore the normal working area of the system is widened under the memristive load.
- (2) At the same time, it can be found that the SIBB converter with the resistive load occurs chaos when $I_{ref} = 5.8$ A, while the SIBB converter with the memristive load occurs chaos when $I_{ref} = 8.9$ A. The point where the chaos occurs moves back significantly, which reduces the probability of chaos of the converter. The eight-period waveform and phase portrait of the converter with the memristive load are shown in Figure 6.
- (3) The behavior of the SIBB converter with the memristive load is much richer. When $I_{ref} \in [9.87, 9.95]$, the system no longer exhibits a chaotic state, but a bifurcation. At this time, the system would occur the tangent bifurcation after chaos [35]. When $I_{ref} = 9.9$ A, the waveform and the phase portrait of i_1 are as shown in Figure 7.

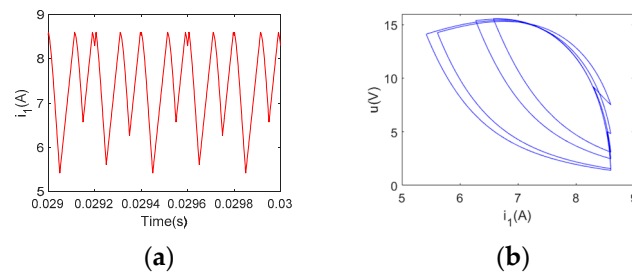


Figure 6. The waveform and phase portrait of i_1 ($I_{ref} = 8.6$ A). (a) The waveform of i_1 , (b) The phase portrait of $u - i_1$.

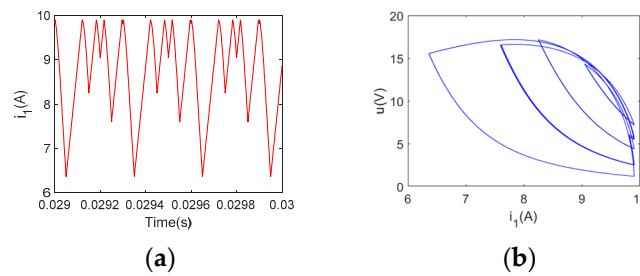


Figure 7. The waveform and phase portrait of i_1 ($I_{ref} = 9.9$ A). (a) The waveform of i_1 , (b) The phase portrait of $u - i_1$.

The bifurcation diagrams of the SIBB converter with the resistive load and memristive load were obtained by MATLAB simulation. Next, the PSIM software was used for simulation to verify the accuracy of the bifurcation and chaotic behavior of the converter with the memristive load.

4. Verification by the PSIM Simulation

The PSIM software is used for simulation to verify the accuracy of the bifurcation and chaotic behavior of the converter with the memristive load. According to the schematic diagram shown in Figure 1, this section builds the simulation model of the system in the PSIM circuit software, as shown in Figure 8. The reference current I_{ref} is selected as the variable, and the parameters of each circuit element are the same as those shown in Table 1. The simulation results of the inductive current i_1 under different states are shown in Figures 9–12.

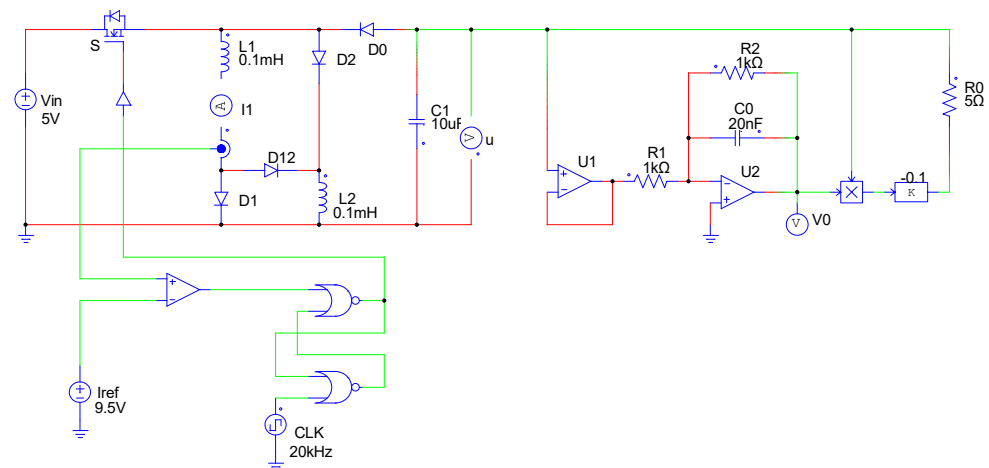


Figure 8. Power simulation (PSIM) diagram.

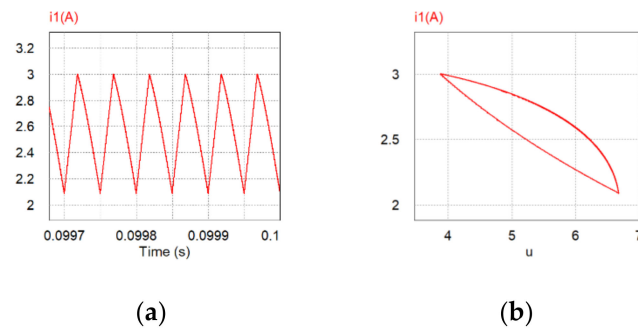


Figure 9. The waveform and phase portrait of i_1 ($I_{ref} = 3$ A). (a) The waveform of i_1 , (b) The phase portrait of $u - i_1$.

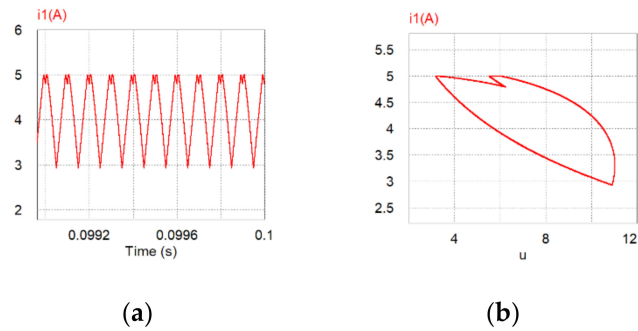


Figure 10. The waveform and phase portrait of i_1 ($I_{ref} = 5$ A). (a) The waveform of i_1 , (b) The phase portrait of $u - i_1$.

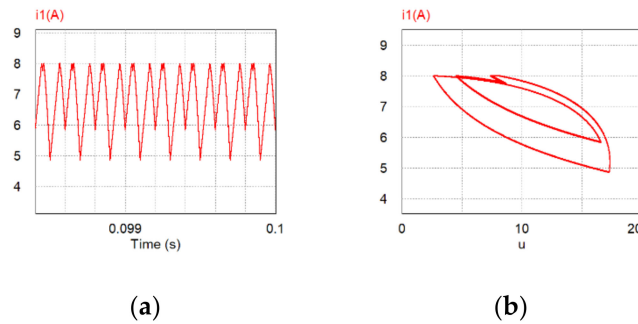


Figure 11. The waveform and phase portrait of i_1 ($I_{ref} = 8$ A). (a) The waveform of i_1 , (b) The phase portrait of $u - i_1$.

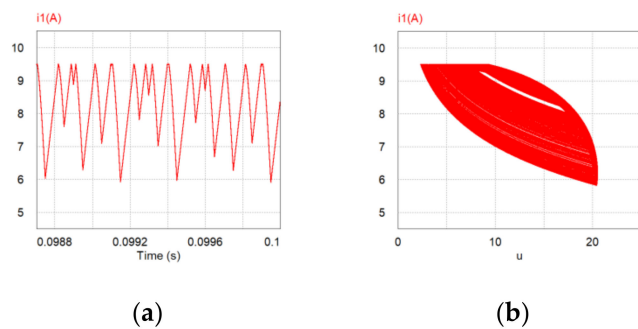


Figure 12. The waveform and phase portrait of i_1 ($I_{ref} = 9.5$ A). (a) The waveform of i_1 , (b) The phase portrait of $u - i_1$.

It can be seen from Figures 9–12 that when I_{ref} is 3.0, 5.0, 8.0, and 9.5 A, the converter is in the state of one-period, two-period, four-period, and chaos, respectively. It is not

difficult to see that the simulation results of this PSIM circuit are consistent with those of the MATLAB simulation.

5. Suppression of the Chaos

The resonant parametric perturbation method takes advantage of the characteristics that the chaotic state is very sensitive to—the minor perturbation of the parameters. By applying certain minor perturbation to the parameters, the system can be controlled from the chaotic state to the stable one-period state.

According to the above results of the PSIM simulation, the SIBB converter with the memristive load is in a chaotic state when $I_{ref} = 9.5$ A. The resonant parametric perturbation method is used to control the chaos of the SIBB converter on this condition.

It is relatively simple that I_{ref} is used as the control parameter. Using $I_{ref2} = I_{ref} + I_{ref1}$ to replace I_{ref} , according to this method, where $I_{ref1} = A \sin(2\pi f t + \varphi)$ and f is the switching frequency ($f = 20$ kHz). Referring to [13], let A equal 0.3 and $\varphi = 1.2$ rad. A minor perturbation is added when $t = 0.05$ s. The circuit diagram of the controller is shown in Figure 13b, compared with the original simple controller in Figure 13a. Then, the waveform of u and i_1 , as well as the phase portrait of $u - i_1$ under the minor perturbation, are obtained, as shown in Figure 14.

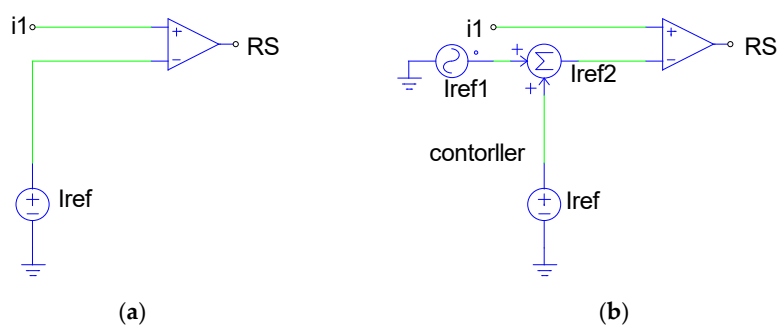


Figure 13. The circuit diagram of the controller. (a) Without perturbation, as in Figure 8, (b) Adding perturbation.

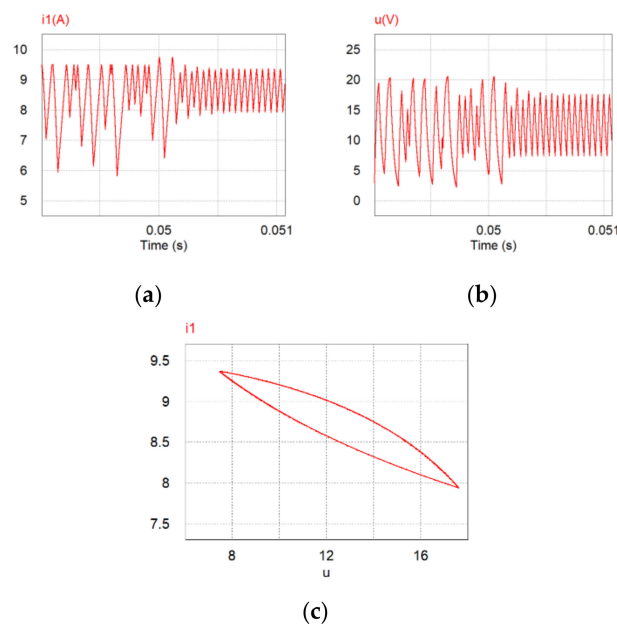


Figure 14. The waveform of u and i_1 , as well as the phase portrait of $u - i_1$ under the minor perturbation. (a) The waveform of i_1 , (b) The waveform of u , (c) The phase portrait of $u - i_1$.

6. Conclusions

In this paper, the nonlinear behavior of the SIBB converter in CCM is observed by using the memristive load instead of the resistive load. In order to study the dynamic effect of the SIBB converter with the memristive load, this paper investigates the working principle of the converter by using the simulation circuit, and obtains the bifurcation diagrams, waveforms, and phase portraits of the inductive current i_1 by controlling the peak current. The results are listed as follows:

- (1) It was found that the system has abundant dynamic behavior, including periodic motion, period-doubling motion, and chaotic motion;
- (2) The memristive load does not affect the bifurcation structure, but expands the normal working area of the system and suppresses the occurrence of chaos;
- (3) At the same time, the SIBB converter with the memristive load has richer behaviors, and appears to demonstrate the behavior of the tangent bifurcation;
- (4) The simulation results of PSIM are consistent with the numerical results of MATLAB. It is also easy to see that the converter has been working in CCM from the waveforms of i_1 ;
- (5) The resonant parametric perturbation method has a good effect on suppressing chaotic phenomenon. The system can be controlled from the chaotic state to the stable one-period state by this method.

In further research, we would extend the memristor model as a nonlinear part into block-oriented nonlinear systems [36–38], to explore the system's performance.

Author Contributions: Conceptualization, methodology, software, validation, formal analysis, investigation, resources, Y.Y., D.L. and D.W.; data curation, D.L.; writing—original draft preparation, writing—review and editing, Y.Y., D.L. and D.W.; supervision, Y.Y. and D.W.; project administration, D.W.; funding acquisition, D.W. All authors have read and agreed to the published version of the manuscript.

Funding: This work was funded by the National Natural Science Foundation of China (no. 61873138), and in part by the Taishan Scholar Project Fund of Shandong Province of China.

Conflicts of Interest: The authors claim that there are no conflicts of interest involved in publishing this article.

References

1. Raghavendra, K.V.G.; Zeb, K.; Muthusamy, A.; Krishna, T.N.V.; Kumar, S.V.S.V.P.; Kim, D.; Kim, M.; Cho, H.; Kim, H. A Comprehensive Review of DC–DC Converter Topologies and Modulation Strategies with Recent Advances in Solar Photovoltaic Systems. *Electronics* **2019**, *9*, 31. [[CrossRef](#)]
2. Singha, A.K.; Kapat, S.; Banerjee, S.; Pal, J. Nonlinear analysis of discretization effects in a digital current mode controlled boost converter. *IEEE J. Emerg. Sel. Top. Circuits Syst.* **2015**, *5*, 336–344. [[CrossRef](#)]
3. Moghaddam, A.F.; van den Bossche, A. Direct Usage of Photovoltaic Solar Panels to Supply a Freezer Motor with Variable DC Input Voltage. *Electronics* **2020**, *9*, 167. [[CrossRef](#)]
4. Lee, M.; Kim, J.; Lai, J. Single inductor dual buck-boost inverter based on half-cycle PWM scheme with active clamping devices. *IET Power Electron.* **2019**, *12*, 1011–1020. [[CrossRef](#)]
5. Saman, A.G.; Mostaan, A.; My, H.T.; Ektesabi, M. Non-isolated buck-boost dc-dc converter with quadratic voltage gain ratio. *IET Power Electron.* **2019**, *12*, 1425–1433.
6. Ajami, A.; Ardi, H.; Farakhor, A. Design, analysis and implementation of a buck-boost DC/DC converter. *IET Power Electron.* **2014**, *7*, 2902–2913. [[CrossRef](#)]
7. Yin, P.; Xia, Z.; Shao, S. Bifurcation and Chaos of Current-Mode Buck-Boost DC-DC Converter. *J. Univ. Shanghai Sci. Technol.* **2013**, *35*, 299–301+306.
8. Demirbaş, Ş.; Fidanboy, H.; Kurt, E. Exploration of the chaotic behaviour in a Buck-Boost converter depending on the converter and load elements. *J. Electron. Mater.* **2016**, *45*, 3889–3899. [[CrossRef](#)]
9. Zhu, B.; Fan, Q.; Li, G.; Wang, D. Chaos suppression for a Buck converter with the memristive load. *Analog Int. Circuits Signal Process.* **2021**. [[CrossRef](#)]
10. Axelrod, B.; Berkovich, Y.; Ioinovici, A. Switched-Capacitor/Switched-Inductor Structures for Getting Transformerless Hybrid DC–DC PWM Converters. *IEEE Trans. Circuits Syst. I* **2008**, *55*, 687–696. [[CrossRef](#)]

11. Liu, H.; Yang, S.; Feki, M. Study on Nonlinear Phenomena in Buck-Boost Converter with Switched-Inductor Structure. *Math. Probl. Eng.* **2013**, *2013*, 1–9. [[CrossRef](#)]
12. Sun, L.; Yang, S.; Liu, H. Bifurcation in discontinuous current-programmed Buck-Boost converter with switched-inductor structure. *J. Harbin Inst. Technol.* **2015**, *47*, 55–61.
13. Tian, L.; Wang, L.; Tao, C. Research on chaos and its control in current-mode switched-inductor converter. *Electr. Drive Locomot.* **2017**, *4*, 36–40.
14. Tian, L.; Qiang, Q.; Tao, C.; Wang, L. Chaos analysis and ramp compensation of switched-inductor buck-boost converter operating in discontinuous conduction mode. *Int. J. Electr. Eng.* **2019**, *26*, 119–126.
15. Wang, N.; Zhang, G.; Bao, H. Bursting oscillations and coexisting attractors in a simple memristor-capacitor-based chaotic circuit. *Nonlinear Dyn.* **2019**, *97*, 1477–1494. [[CrossRef](#)]
16. Levy, Y.; Bruck, J.; Cassuto, Y.; Friedman, E.G.; Kolodny, A.; Yaakobi, E.; Kvatinisky, S. Logic operations in memory using a memristive Akers array. *Microelectron. J.* **2014**, *45*, 1429–1437. [[CrossRef](#)]
17. Li, B.; Zhao, Y.; Shi, G. A Novel Design of Memristor-based Bidirectional Associative Memory Circuits Using Verilog-AMS. *Neurocomputing* **2018**, *330*, 437–448. [[CrossRef](#)]
18. Zhang, P.; Li, C.; Huang, T.; Chen, L.; Chen, Y. Forgetting memristor based neuromorphic system for pattern training and recognition. *Neurocomputing* **2017**, *222*, 47–53. [[CrossRef](#)]
19. Duan, S.; Hu, X.; Dong, Z.; Wang, L.; Pinaki, M. Memristor-based cellular nonlinear/neural network: Design, analysis, and applications. *IEEE Trans. Neural Netw. Learn. Syst.* **2015**, *26*, 1202–1213. [[CrossRef](#)]
20. Kim, S.J.; Kim, S.B.; Jang, H.W. Competing memristors for brain-inspired computing. *iScience* **2020**, *24*, 101889.
21. Owlia, H.; Keshavarzi, P.; Rezai, A. A novel digital logic implementation approach on nanocrossbar arrays using memristor-based multiplexers. *Microelectron. J.* **2014**, *45*, 597–603. [[CrossRef](#)]
22. Vourkas, I.; Sirakoulis, G.C. Memristor-based combinational circuits: A design methodology for encoders/decoders. *Microelectron. J.* **2014**, *45*, 59–70. [[CrossRef](#)]
23. Bao, H.; Wang, N.; Bao, B.; Chen, M.; Jin, P.; Wang, G. Initial condition-dependent dynamics and transient period in memristor-based hypogenetic jerk system with four line equilibria. *Commun. Nonlinear Sci. Numer. Simul.* **2018**, *57*, 264–275. [[CrossRef](#)]
24. Bao, B.; Wang, N.; Xu, Q.; Wu, H.; Hu, Y. A simple third-order memristive band pass filter chaotic circuit. *IEEE Trans. Circuits Syst. II: Express Briefs* **2017**, *64*, 977–981. [[CrossRef](#)]
25. Dou, G.; Duan, H.; Yang, W.; Yang, H.; Guo, M.; Li, Y. Effects of Initial Conditions and Circuit Parameters on the SBT-Memristor-Based Chaotic Circuit. *Int. J. Bifurc. Chaos* **2019**, *29*, 17. [[CrossRef](#)]
26. Guo, M.; Gao, Z.; Xue, Y.; Dou, G.; Li, Y. Dynamics of a physical SBT memristor-based Wien-bridge circuit. *Nonlinear Dyn.* **2018**, *93*, 1681–1693. [[CrossRef](#)]
27. Shin, S.; Kim, K.; Kang, S. Memristor applications for programmable analog ICs. *IEEE Trans. Nano-Technol.* **2011**, *10*, 266–274. [[CrossRef](#)]
28. Zidan, M.A.; Jeong, Y.; Shin, J.H.; Du, C.; Zhang, Z.; Lu, W.D. Field-Programmable Crossbar Array (FPCA) for Reconfigurable Computing. *IEEE Trans. Multi-Scale Comput. Syst.* **2018**, *4*, 698–710. [[CrossRef](#)]
29. Hong, Y.; Lian, Y. A memristor-based continuous-time digital FIR filter for biomedical signal processing. *IEEE Trans. Circuits Syst. I: Regul. Pap.* **2015**, *62*, 1392–1401. [[CrossRef](#)]
30. Yu, Y.; Yang, N.; Yang, C.; Tashi, N. Memristor bridge-based low pass filter for image processing. *J. Syst. Eng. Electron.* **2019**, *30*, 448–455. [[CrossRef](#)]
31. Hua, M.; Yang, S.; Xu, Q.; Chen, M.; Wu, H.; Bao, B. Forward and reverse asymmetric memristor-based jerk circuits. *AEUE Int. J. Electron. Commun.* **2020**, *123*, 153294. [[CrossRef](#)]
32. Zhang, R.; Wu, A.; Zhang, S.; Wang, Z.; Cang, S. Dynamical analysis and circuit implementation of a DC/DC single-stage boost converter with memristance load. *Nonlinear Dyn.* **2018**, *93*, 1741–1755. [[CrossRef](#)]
33. Bao, B.; Zhang, X.; Bao, H.; Wu, P.; Wu, Z.; Chen, M. Dynamical effects of memristive load on peak current mode buck-boost switching converter. *Chaos Solitons Fractals* **2019**, *122*, 69–79. [[CrossRef](#)]
34. Bao, B. *An Introduction to Chaotic Circuits*; Science Press: Beijing, China, 2013.
35. Zhou, Y.; Chen, J. Tangent bifurcation and intermittent chaos in current-mode controlled BOOST converter. *Chin. J. Electr. Eng.* **2005**, *25*, 26–29.
36. Wang, D.; Zhang, S.; Gan, M.; Qiu, J. A novel EM identification method for Hammerstein systems with missing output data. *IEEE Trans. Ind. Inform.* **2020**, *16*, 2500–2508. [[CrossRef](#)]
37. Wang, D.; Li, L.; Ji, Y.; Yan, Y. Model recovery for Hammerstein systems using the auxiliary model based orthogonal matching pursuit method. *Appl. Math. Model.* **2018**, *54*, 537–550. [[CrossRef](#)]
38. Wang, D.; Yan, Y.; Liu, Y.; Ding, J. Model recovery for Hammerstein systems using the hierarchical orthogonal matching pursuit method. *J. Comput. Appl. Math.* **2019**, *345*, 135–145. [[CrossRef](#)]